JOURNAL OF MATERIALS SCIENCE **34** (1999) 1073–1079

AES study of passive films formed on a type 316 austenitic stainless-steels in a stress field

F. NAVAÏ*, O. DEBBOUZ
Laboratoire de Génie des Matériaux, ISITEM, Université de Nantes, La Chantrerie, C.P. 3023, 44087 Nantes Cedex 03, France

The type AISI 316 stainless steel, in addition to the principal alloying elements chromium and nickel, contains 2.5–3.5% of molybdenum. This element is added to improve the mechanical properties and the pitting resistance of austenitic alloys. Concerning the Stress Corrosion Cracking (SCC) resistance of austenitic stainless steels, molybdenum additions to alloys have a variable effect: the effect is detrimental for small additions of Mo, and it is beneficial for the alloy containing more than 4% Mo. Thus the Mo concentration on passive film plays an important role on the SCC resistance of steels. On the other hand, in a previous investigation, it was shown that the composition of passive films formed on the stressed 302 alloy depended on the compressive or tensile nature of stresses. Consequently, the aim of the present work is to study the composition of passive films formed on 316 steel and the migration of molybdenum in a stress field. Thus, Auger electron spectroscopy spectra were recorded to determine the chemical composition of the passive films formed on both sides of the type AISI 316 stainless steel U-bend samples. The results obtained show that the behaviour of chromium and oxygen in passive films formed on 316 steel in the stress field was nearly similar to that formed on 302 steel. Concerning the molybdenum diffusion outwards the passive film formed on the 316 steel was reduced by either the tensile or compressive stress field.

1. Introduction

Generally, molybdenum added to stainless steels increases their passivating ability and decreases the activity of the weak points of the passive films. Consequently, molybdenum assists passivation of the stainless steels but does not constitute the passive film. When passivity failure occurs at weak points of passive film, the localized active dissolution of all the alloy constituents leads to a corrosion product film formation, in which molybdenum ions are significantly concentrated.

The molybdenum enriched corrosion product film is due probably to the fact that molybdenum is passive in the active region of chromium and iron. It acts as an effective diffusion barrier against further active dissolution of the alloy [1–2]. Vanslembrouck *et al.* [3] studied the behaviour of several austenitic stainless steels in neutral chloride solutions. They found that the molybdenum presence improves the resistance of steels against pitting attack.

Cieslak *et al.* [4] found also a beneficial effect of alloyed molybdenum. However, Latanision and Staehle [5–6] suggested that molybdenum has a variable effect on the stress corrosion cracking (SCC) resistance of austenitic stainless steels. Above 5%, the effect is beneficial, while below 5% it is rather detrimental.

In this way, Loginow and Bates [7] have shown that a small addition of molybdenum (0.1%) to a 18Cr-8Ni steel exposed to $MgCl_2$ solutions had a detrimental effect on the failure time of this steel. Kowaka and Fujikawa [8] found identical results. On the contrary, Staehle *et al.* [9], and Desesteret and Wagner [10], found that somewhat larger percentages of Mo in stainless steels tested still had a detrimental effect.

Concerning the effect of cold work on the corrosion resistance of alloys, many papers shown that cold work decreases the ability to passivate the austenitic stainless steels [11].

Cigada *et al.* [12] correlated the SCC resistance reduction to an increase in concentration of internal micro-stresses. Hawkes *et al.* [13] showed that the cold work stretching effect on stress corrosion cracking of type 316 stainless steel was deleterious by boiling magnesium chloride solution. On the contrary, there are some indications showing that beneficial effects of cold work could be observed [14–15]. This is mainly, the case for cold rolling or extrusion, which produce compressive residual stresses and enhance the resistance of the samples to aggressive environments.

Concerning the effect of the compressive stress on the corrosion resistance of stainless steels, it has been shown in a previous investigation [16], that the composition of passive films formed under stress on 302 alloy depended on compressive or tensile nature of stresses. It was also shown that the beneficial effects

* Author to whom all correspondence should be addressed.

of compressive stress was both related to the increasing chromium enrichment and the decreasing thickness of the passive film.

2. Experimental

2.1. Base material

Rectangular specimens of 100 mm long, 8 mm wide and 0.25 mm thick, investigated in the present study were cut from a type 316 stainless steel sheets from Goodfellow, supplied in a ductile pure austenitic structure state (annealed at 1050 °C and quenched). The longitudinal axes of the samples were oriented parallel to the prior rolling direction of the sheet. The chemical composition of the investigated steel is given in Table I.

Fig. 1 presents the stress-strain curve of the investigated base material, where elastic and plastic domains are clearly shown. It can be noticed that the offset yielding point is about 300 MPa and the ultimate tensile strength is ≈625 MPa corresponding to a failure strain of 0.49 mm/mm.

2.2. Surface pretreatment

After cutting the sheets to rectangular specimens, the tested samples received the following initial preparation.

They were washed with soap, rinsed with water, and ultrasonically degreased in an acetone bath. They were then electropolished for 3 minutes with a current density of 1 A cm^{-2}, in a 15% sulphuric acid (R.P. Normapur, 95% minimum, $d = 1.83$) and 85% orthophosphoric acid (R.P. Normapur, 85% minimum, $d = 1.70$) mixture at temperature 35 °C. The samples were then washed in doubly distilled water, and finally dired in a hot air flow.

2.3. Mechanical stressing

Before immersing in the acidic bath, the samples (excepted R sample) were subjected to a loop test. They were first plastically deformed into a U-shape at a curvature radius of $\rho = 7 \pm 0.25$ mm (Fig. 2a), then the two extremities were clamped together in order to add the elastic stress (Fig. 2b).

The superficial stress due to the bending of the specimen is estimated to be slightly higher than the base material yielding point (about 350 MPa). Table II indicates the maximum external stress in the outer layers of the U-bend sample. For a realistic comparison, an unstressed sample, denoted R, was prepared and studied as a reference specimen.

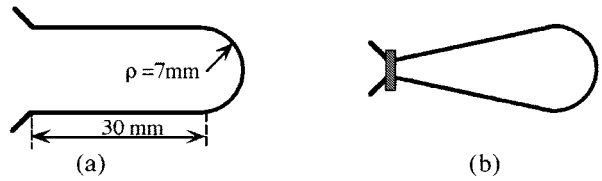

Figure 2 Mechanical straining of sample: (a) rolled specimen plastically deformed before stressing; (b) stressed specimen after adding the elastic stress.

TABLE I Chemical composition of the investigated steel (wt %)

Composition (%)							
Cr	Ni	Mn	Mo	C	S	P	Fe
16–20	8–14	<2	2.5–3.5	<0.12	<0.03	<0.045	Balance

TABLE II Strain and stress of U-bend specimen

Sample	Radius of curvature (mm)	Strain (mm/mm)	Estimation of stress (MPa)
U-bend	7 ± 0.5	≥0.02	Residual ± 350
R	∞	0	Residual

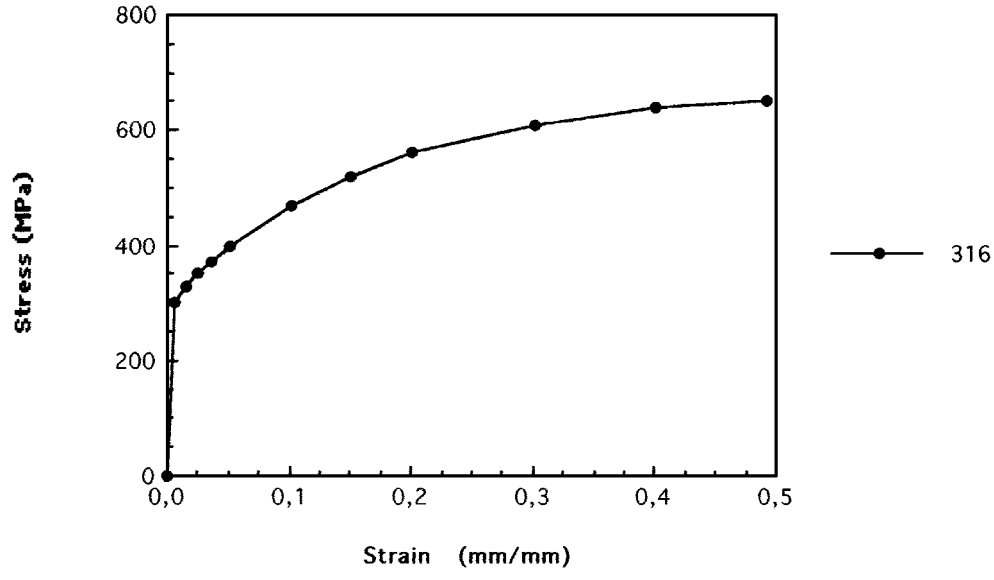

Figure 1 Stress strain-curve for 316 stainless steel, straining rate $\varepsilon^{\circ} = 1.39\ 10^{-3}\ s^{-1}$.

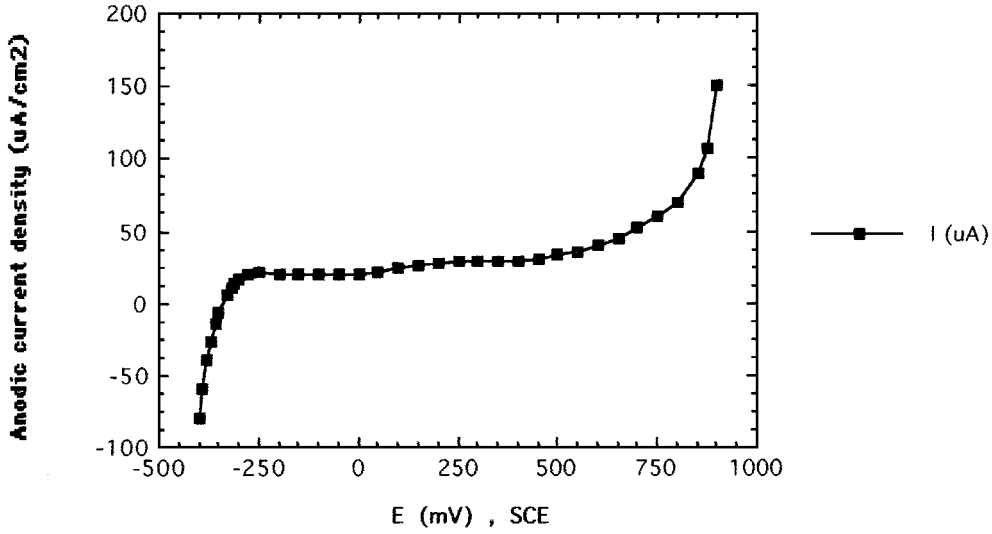

Figure 3 Potentiodynamic polarization curve for the type 316 stainless steel in 1 N sulphuric acid. Sample potential were measured against the satured calomel electrode (SCE).

3. Results and discussion

3.1. Polarization curves

In order to determine the passivation potential domain, anodic potentiodynamic measurements, were done on the unstrained sample at a scanning rate of 100 mV min^{-1} and the current density versus potential is recorded. These measurements were conducted by placing the samples as the working electrode, in the presence of a platinum electrode and a saturated calomel reference electrode (SCE) in the electrolyte.

The results in Fig. 3 show that the passivation domain ranges from about -250 mV to nearly $+900$ mV, with a minimum current of 19 μA at -150 mV/SCE. However, the passivation potential of $+450$ mV, for which the anodic current is about 31 μA and the passive layer is more stable, was chosen as an electrode potential in the potentiostatic tests to study the passivation kinetics of the samples. It can be noticed from the polarization curve that the passivation critical current peak is absent. This signifies that this alloy is easily passivated in normal sulphuric acid solution.

3.2. Passivation of the samples

After the initial preparation, each tested sample was quickly immersed in 1N H_2SO_4 solution. Then, in order to eliminate the thin oxide film formed on the sample surface between the end of the electropolishing and its introduction into the bath, the sample was first cathodically pretreated at -550 mV/SCE. The cathodization was stopped when the current density reached the value of -200 μA cm^{-2}, and then, the anodization treatment was begun. Each sample was passivated under a voltage of $+450$ mV/SCE during 20 minutes, at room temperature. The stable passive layers grown on the sides of the tested samples were studied subsequently by means of Auger electron spectroscopy (Vacuum Generators).

3.3. Surface physical analysis

After anodization, the samples were immediately rinsed in water, dried in air flow, and then introduced into an Auger electron spectrometer, where the composition depth profiles measurements were carried out. The AES analysis were, in addition of unstrained sample, done on both compressive and tensile strained surfaces of samples.

The elemental depth profiling was obtained from a series of repeated cycles of argon ion abrasion and AES analyses. The results were plotted from the peak-to-peak heights of the principal Auger lines against the ion milling time (Fig. 4). Each ion abrasion time period was fixed to 60 seconds, corresponding to the removal of approximately 0.48 nm of silicon. Error estimation is not reported on the figures for better clarity and it ranges from 2 to 4%.

The peak-to-peak heights of the principal Auger lines (the 703 eV Fe line, the 529 eV Cr line, the 848 eV Ni line, the 510 eV O line, and the 272 eV C line) are plotted against the ion milling time in Fig. 4. The carbon and sulphur peak are not reported for clarity. In fact, the concentration of sulphur in the alloy is very low ($<0.03\%$) and that of carbon is less than 0.16% and does not seem to influence significantly the passive layer [7–9]. It has previously been shown that the presence of sulphur in passive film is principally due to bath contamination and that of the carbon results from external contamination produced due to exposure to CO_2 from the atmosphere [16].

The study of iron AES depth concentration profiles of the passive film is important, because iron is not only the principal constituent of steels, but also its peak is usually used to determine the ratios of the Auger peak heights of the alloying elements.

As it can be seen from Fig. 5, the iron concentration of the passive film is substantially weak in the outer layer of passive film, its Auger line intensity increases strongly with the increasing depth. The Fe_{bulk}/Fe_{film} ratio varies from 1 to 5. It was shown previously that the iron impoverishment of the passive film was rather due to the higher diffusion rate of chromium than the iron preferential dissolution [17, 18]. In fact, this phenomena is also observed in the case of dry oxidation, where the dissolution of all elements is excluded. For

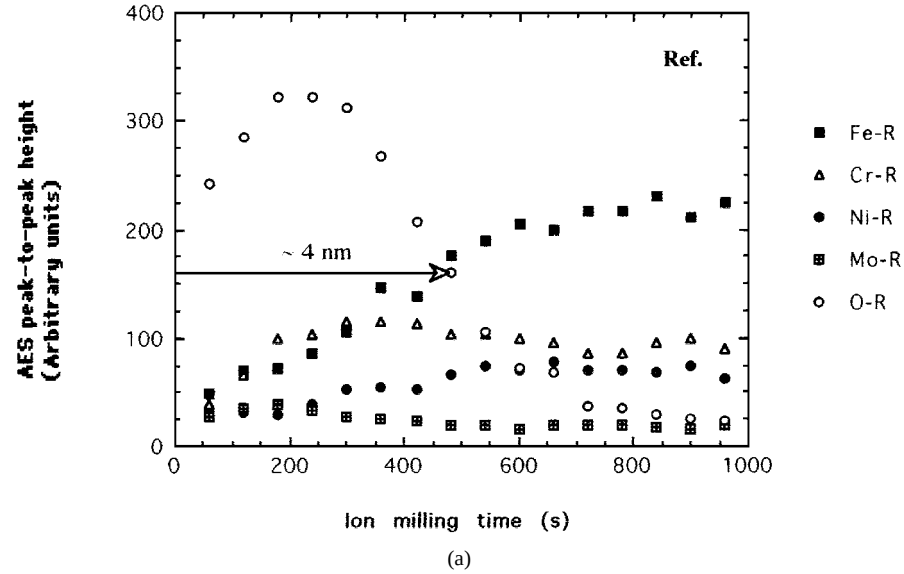

(a)

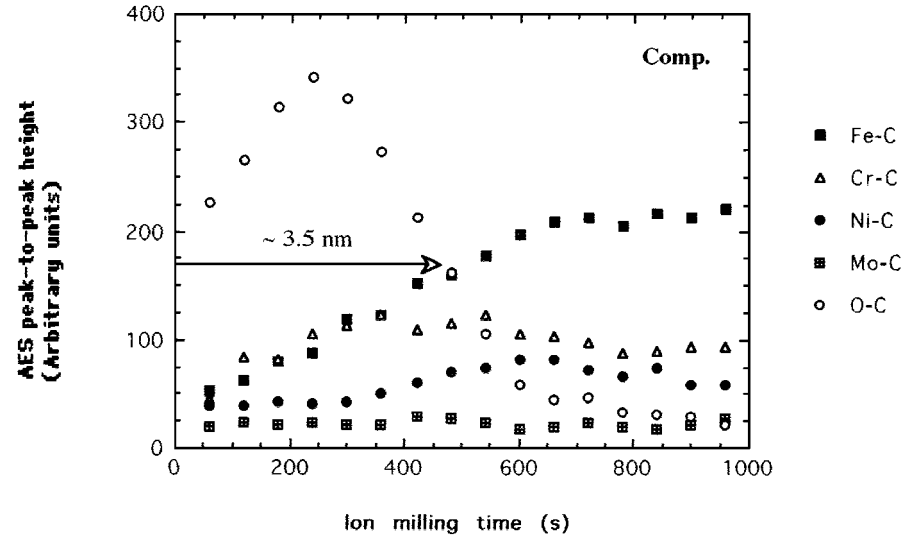

(b)

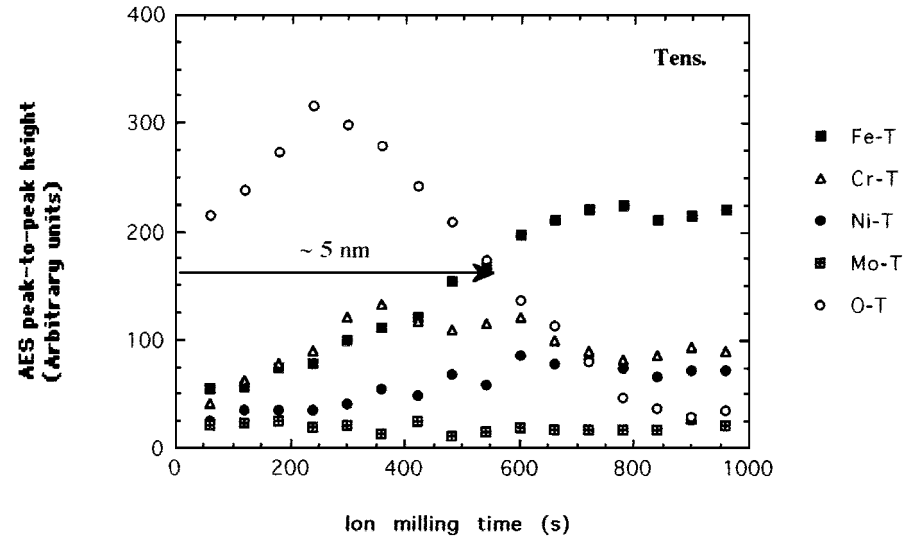

(c)

Figure 4 AES depth concentration profiles of the passive film formed on Type 316 steel specimens in 1N H_2SO_4 solution. The profiles were measured on (a) reference sample, (b) the compressive strained side of the sample, (c) the tensile strained side of the same sample.

example, the Cr(529 eV)/Fe(703 eV) pronounced dependence ratio for the oxide films formed on a 302 stainless steel during an oxidation of 45 minutes (at a temperature of 928 K under an oxygen partial pressure of about 0.2 Pa), indicated that there is an important selective enrichment in chromium with a maximum value of 4.6 for the compressive strained side [19].

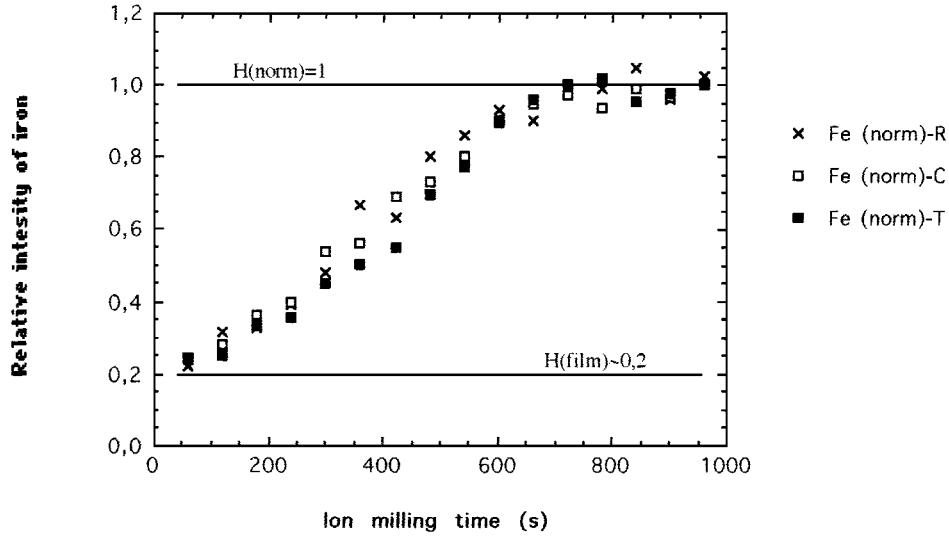

Figure 5 Normalized iron AES depth concentration profiles of the passive film formed on the compressive, tensile and non strained sides of samples.

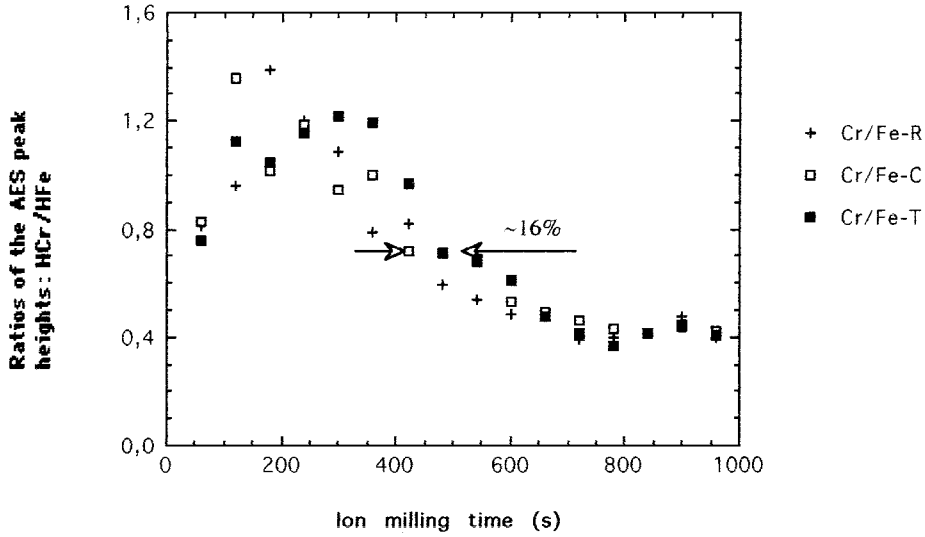

(a)

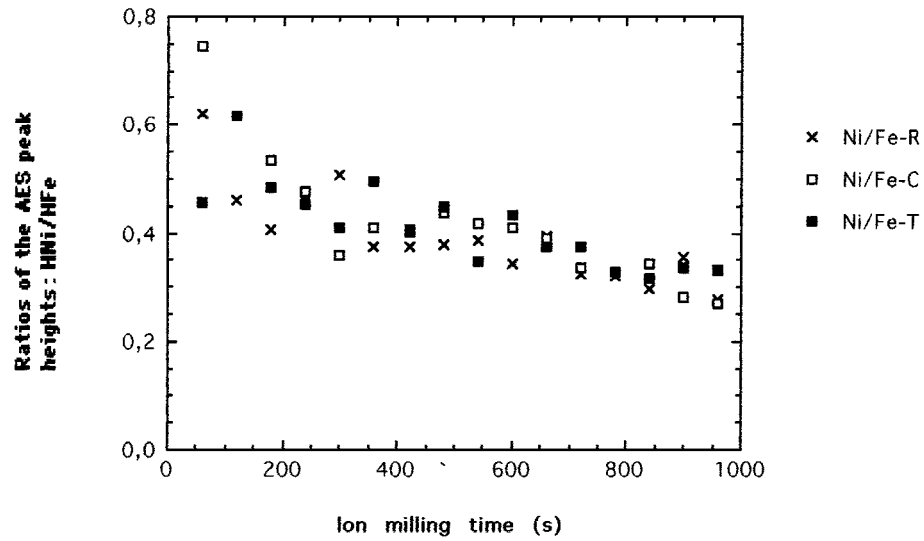

(b)

Figure 6 Ratios of the Auger peak heights (a): Cr(529 eV)/Fe(703 eV), (b): Ni(848 eV)/Fe(703 eV), (c): Mo(eV 186)/Fe(703 eV) and (d): O(510 eV)/Fe(703 eV) as a function of the ion milling time for the R sample and compressive and tensile strained sides.

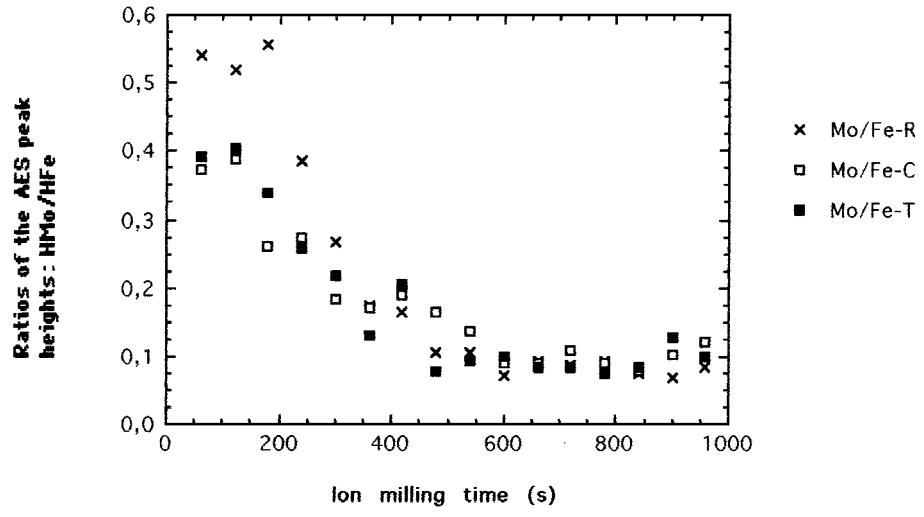

(c)

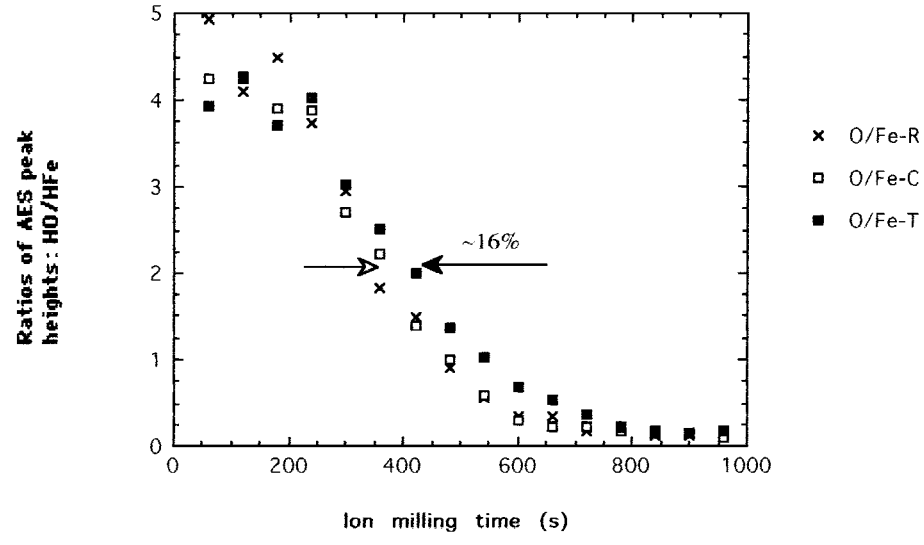

(d)

Figure 6 (*continued*)

According to the Fig. 4a, b and c, it can be observed that, in general, the passive film region was relatively enriched in chromium and depleted in nickel. In addition, these figures show also that the chromium enriched layer due to the chromium migration outwards through the passive film, is followed by a chromium depletion region. This depletion occurred only at high depth where the chromium content reaches its bulk value.

Fig. 6a and b present the Auger peaks heights ratio changes of Cr(529 eV)/Fe(703 eV) and Ni(848 eV)/Fe(703 eV) of all samples as a function of the ion milling time. From Fig. 4b–c, it can be observed that the width of the region affected by the chromium enrichment is greater on the tensile strained surface than it is on the compressive strained one. The Cr(529 eV)/Fe(703 eV) ratio indicates also that there is a selective enrichment of chromium, because of its migration towards the oxide film (Fig. 6a). Moreover, according to the Ni(848 eV)/Fe(703 eV) ratio depth profile (Fig. 6b), it is shown that there is also a selective enrichment of nickel. The real concentration of nickel, as it was mentioned above, is depleted in the passive film, nevertheless a Ni enrichment can be observed in métal/film interface (~5.5 nm) (Fig. 4a, b, c). Consequently, the selective enrichment of nickel in this region is rather due to the iron concentration decrease in passive film (cf. Fig. 5).

Concerning the supplementary alloying element molybdenum, as can be seen from Fig. 4a, the reference sample passive film is relatively enriched in molybdenum. This enrichment disappears after an ion milling time of about 500 s (~4 nm). On the contrary, the tensile strained film is impoverished in this elements, but less than the compressive strained side (Fig. 4b, c). The depletion of this element occurred at high depth (about 5–7 nm). Similarly and according to the Fig. 6c, the Mo(186 eV)/Fe(703 eV) ratio point out a selective enrichment of molybdenum, for the reference sample, R. Concerning the tensile and compressive strained sides of samples, Fig. 6c shows that, in a stress field, whatever the nature of stress, the Mo/Fe ratios are reduced in outer layers of passive film. However, the Mo/Fe ratio of tensile stressed side remains slightly higher than the ratio of compressive strained side.

AES depth profiles for oxygen show (see Fig. 4a, b, c) a similar effect of the stress field on the passive layer growth. This effect was already observed in the case of 302 stainless steel: the passive layer of non-stoichiometric formula is richer in oxygen and more thicker on the tensile strained surfaces than it is on the unstrained or the compressive strained one [16]. But, in the present investigation, the width difference between the tensile and compressive sides of the 316 steel, is less than the case of 302 alloy. This is probably due to the yield stress of 316 steel (≅300 MPa), in comparison with 302 steel (≅900 MPa). Fig. 4b and c show the Auger peak height change of oxygen, O(510 eV), as a function of the ion milling time. This value indicates that the increase in relative depth of the oxide thickness is about:

$$(d_{\text{tens}} - d_{\text{comp}})/d_{\text{comp}} \approx 16\%$$

where d_{tens} and d_{comp} are the average thickness of oxide films formed on tensile and compressive sides of specimen, respectively.

4. Conclusion

The results obtained in this investigation allow the following conclusions to be drawn:

1. The passive layer formed on 316 stainless-steel in sulphuric acid is thicker on the tensile strained surface than it is on the compressive strained one or on the reference sample.
2. The apparent thickness of the oxide film, developed on the unstrained sample, was found to be similar to that formed on the compressive stressed side, and greater than that formed on the tensile stressed one.
3. The molybdenum concentration in the outer layers of passive films is higher on the unstressed sample than it is on the compressive or tensile stressed sides. Consequently, the molybdenum migration outwards in passive film was reduced in a stress field, whatever the tensile or compressive nature of stresses.

References

1. K. ASAMI, M. NAKA, K. HASHIMOTO and T. MASUMOTO, *J. Electrochem. Soc.* **127** (1980) p. 2130.
2. K. HASHIMOTO, in "Passivity of Metals and Semiconducteurs," edited by M. Froment (Elsevier Science Publishers B. V. Amesterdam, 1985) p. 246.
3. P. VANSLEMBROUCK, W. BOGARTS and A. VAN HAUTE, *ibid.* p. 393.
4. W. R. CIESLAK and D. J. DUQUETTE, *ibid.* p. 405.
5. R. M. LATANISION and R. W. STAEHLE, "Fondamental Aspects of Stress Corrosion Cracking," edited by R. W. Staehle, A. J. Forty and D. Van Rooyen (NACE, Houston, 1969) p. 214.
6. "Stress Corrosion Cracking and Hydrogen Embrittlement of Iron Base Alloys" (NACE 5, Unieux Firminy, 1973 & 1977).
7. A. W. LOGINOW and J. F. BATES, "Influence of Alloying Elements on the Stress Corrosion Behaviour of austenitic Stainless Steels," (NACE Conference, Cleveland, Ohio, 1968), preprint.
8. M. KOWAKA and J. FUJIKAWA, *The Sumitomo Search* **7** (1972) 10.
9. R. W. STAEHLE, J. J. ROYUELA, T. L. RAREDON, E. SERRATE, C. R. MORIN and R. V. FARRAR, *Corrosion*, **26** (1970) 451.
10. A. DESESTERET and G. H. WAGNER, *Werkst. Korro.* **20** (1969) 300.
11. W. D. FRANCE, Jr., *Corrosion NACE* **26** (1970) 189.
12. A. CIGADA, N. MAZZA, P. PEDEFERRI, G. SALVAGO, D. SINIGALALIA and G. ZANNI, *Corr. Sci.* **23** (1983) 195.
13. H. P. HAWKES, F. H. BECK and M. G. FONTANA, *Corrosion NACE* **9** (1963) 247t.
14. J. C. CHARBONNIER. *Mémoires et Etudes Scientifiques Revue de Métallurgie* **3** (1981) 121.
15. H. L. LOGAN and M. J. McBEE, Materials Research and Standards, ASTM Special Technical Publication 264, Case History No. 49. (1961) p. 38.
16. F. NAVAÏ, *J. Mater. Sci.* **30** (1995) 1166.
17. A. CIGADA, *Corr. Sci.* **22** (1982) 559.
18. J. C. LANGEVOORT, T. FRANSEN and P. J. GELLINGS, *Werkstoffe und Korrosion* **34** (1983) 50.
19. F. NAVAÏ, Thesis, ISITEM, Université de Nantes, 1997.

Received 28 August 1997
and accepted 8 October 1998